Modes splitting in graphene-based double-barrier waveguides*

Si-Pu You(有四普), Ying He(何英)†, Yan-Fang Yang(杨艳芳), and Hui-Fang Zhang(张惠芳)

Department of Physics, College of Sciences, Shanghai University, Shanghai 200444, *China*

(Received 28 June 2016; revised manuscript received 17 November 2016; published online 13 February 2017)

The graphene-based double-barrier waveguides induced by electric field have been investigated. The guided modes can only exist in the case of Klein tunneling, and the fundamental mode is absent. The guided modes in the single-barrier waveguide split into symmetric and antisymmetric modes with different incident angles in the double-barrier waveguide. The phase difference between electron states and hole states is also discussed. The phase difference for the two splitting modes is close to each other and increases with the order of guided modes. These phenomena can be helpful for the potential applications in graphene-based optoelectronic devices.

Keywords: graphene, double-barrier waveguides, modes splitting

PACS: 03.65.Pm, 05.60.Gg, 94.05.Pt, 41.75.Fr **DOI:** 10.1088/1674-1056/26/3/030301

1. Introduction

In recent years, more and more research on graphene has been done experimentally and theoretically[1–6] due to its remarkable properties and potential applications.[7–11] Graphene is a single two-dimensional layer of carbon atoms bound in a hexagonal lattice structure, and the quasi particle exactions around the Dirac point obey a linear Dirac-like energy dispersion law, which can be described by a two-dimensional Dirac equation.[8] It exhibits many unique properties.[12–21]

As we all know, quasiparticles in graphene exhibit the linear dispersion relation, which is similar to that of light or photons. Thus it is possible to make an analogy between the propagation of electron waves in a graphene waveguide and electromagnetic waves in dielectric optical waveguides. Electrons in graphene near the Dirac point exhibit some optical-like phenomenon, such as reflection, refraction, and transmission. Moreover, the electrons in graphene have very long mean free paths and seem to be almost insensitive to disorder and electron–electron interactions.[7] Hence, quantum well or barrier in graphene can act as a slab waveguide for electrons wave.[22–28]

It is necessary to compare the difference between an optical waveguide and a graphene waveguide. First, the guided modes in an optical waveguide depend on the configuration of the waveguide and the material properties of the guiding film, the cover, and the substrate. For a graphene waveguide, the layers are characterized by potential energies, which can be modulated by the external electric field without changing the configuration of the waveguide. Secondly, in the graphene waveguide the guided modes are generated due to the propagation of ballistic electrons governed by the Dirac-like equation, while in the dielectric optical waveguide the guided modes are generated due to the propagation of electromagnetic waves satisfying the Helmholtz equation. Many achievements about graphene waveguides have been reported.[24–34] The waveguide induced by a δ-function-like magnetic field exhibits a step-like increase in conductance with increasing fermion energy.[23] The graphene-based waveguide with electrostatic potential modulation and magnetic modulation by ferromagnetic stripes has been investigated.[24–28,35] All of these results show that the characteristics of the guided modes differ due to the different modulation method and different waveguide structures.

The research about graphene-based waveguides mainly focuses on the quantum well structures,[24–27,36] while only a small part of potential barrier structures have been studied.[28,37–39] The graphene waveguide with a single barrier structure has been studied in detail.[28] In the graphene-based double-barrier structures, the giant Goos–Hänchen shift, resonant tunneling, and shot noise have been reported,[37–39] which demonstrate some different properties compared with that in the single barrier structure. The graphene double-barrier structure is an important field, since practical optoelectronic devices are not made of simple structures such as a single quantum barrier or a single quantum well while it may consist of double barriers or double wells. Moreover, the graphene waveguide with a double-barrier structure possesses more extensive physical phenomena than those in the single-barrier structure.

Here we will investigate the guided modes in a graphene-based double-barrier waveguide. The results show that guided modes in double-barrier waveguides will split. The splitting of guided modes is very sensitive to well widths and barrier heights. When the well width, which is the distance in-

*Project supported by the National Natural Science Foundation of China (Grant Nos. 11204170 and 61108010) and the Shanghai Municipal Commission of Science and Technology, China (Grant No. 16ZR1411600).

†Corresponding author. E-mail: heying@staff.shu.edu.cn

© 2017 Chinese Physical Society and IOP Publishing Ltd

terval between two barriers, tends to be large enough, impact between the two barriers will be ignored, and thus the double-barrier waveguides will degenerate into two single barrier waveguides. The phase difference between electron states and hole states has also been discussed and the relationship between the phase difference and the order of guided modes is also illustrated.

2. Model and theory

In this work, we consider the symmetric double-barrier waveguides induced by monolayer graphene, as shown in Fig. 1. A graphene-based barrier can be created with two electrostatic gates, a global back gate, and a local top gate, applying on the sheet of graphene. The potential profiles of the five zones of the double-barrier waveguides are denoted by

$$V_1(x) = \begin{cases} V_0, & 0 \le x \le x_1, x_2 \le x \le x_3, \\ 0, & \text{otherwise.} \end{cases} \tag{1}$$

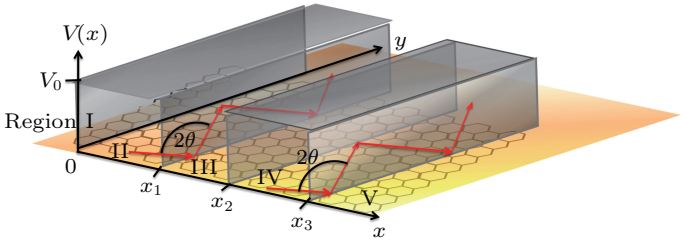


Fig. 1. (color online) Schematic structure of the double-barrier waveguides based on graphene.

In Fig. 1, θ is the incident angle with respect to the x axis, and the propagation direction of the guided modes is the y axis. The double-barrier waveguides we consider here are induced by electrostatic field, and we can control the height of barriers by changing the strength of electrostatic field.

The low energy band structure for a single valley (K lattice point) in graphene can be described by the 2D Dirac-like Hamiltonian

$$[-\mathrm{i}\hbar v_\mathrm{F}(\boldsymbol{\sigma}\cdot\boldsymbol{\nabla}) + V(x)]\psi = E\psi, \tag{2}$$

where $v_\mathrm{F} \approx 10^6$ m/s is Fermi velocity, $\boldsymbol{\sigma} = (\sigma_x, \sigma_y)$ are the Pauli matrices, E is the incident energy of electron, and $\hbar$ is Planck's constant h divided by 2π. Since a graphene honeycomb lattice contains two sublattices A and B, $\phi(x)$ can be expressed by a two component spinor, i.e., $\phi(x) = [\phi^\mathrm{A}(x), \phi^\mathrm{B}(x)]$, where $\phi^\mathrm{A}(x)$ and $\phi^\mathrm{B}(x)$ represent the smooth enveloping functions of sublattices A and B, respectively. As a result of translation invariance in the y direction, $\psi(x,y)$ can be written as $\psi(x,y) = \phi(x)\,\mathrm{e}^{\mathrm{i}k_y y}$. Thus we can obtain

$$\frac{\mathrm{d}\phi^\mathrm{A}(x)}{\mathrm{d}x} - k_y\phi^\mathrm{A}(x) = \mathrm{i}\frac{E - V(x)}{\hbar v_\mathrm{F}}\phi^\mathrm{B}(x), \tag{3a}$$

$$\frac{\mathrm{d}\phi^\mathrm{B}(x)}{\mathrm{d}x} + k_y\phi^\mathrm{B}(x) = \mathrm{i}\frac{E - V(x)}{\hbar v_\mathrm{F}}\phi^\mathrm{A}(x). \tag{3b}$$

The solution to Eq. (3) for a given energy in the five regions can be written as

$$\phi^\mathrm{A}(x) = \begin{cases} A\,\mathrm{e}^{\alpha x}, & x < 0, \\ B\cos(k_x x) + C\sin(k_x x), & 0 < x < x_1, \\ A'\,\mathrm{e}^{\alpha(x-x_2)} + D\,\mathrm{e}^{-\alpha(x-x_1)}, & x_1 < x < x_2, \\ B'\cos[k_x(x-x_2)] + C'\sin[k_x(x-x_2)], & x_2 < x < x_3, \\ D'\,\mathrm{e}^{-\alpha(x-x_3)}, & x_3 < x, \end{cases} \tag{4a}$$

$$\phi^\mathrm{B}(x) = \begin{cases} \mathrm{i}S'[A(k_y - \alpha)\,\mathrm{e}^{\alpha x}]/k_2, & x < 0, \\ \mathrm{i}S[(Bk_y - Ck_x)\cos(k_x x) + (Bk_x + Ck_y)\sin(k_x x)]/k_1, & 0 < x < x_1, \\ \mathrm{i}S'[A'(k_y - \alpha)\,\mathrm{e}^{\alpha(x-x_2)} + D(\alpha + k_y)\,\mathrm{e}^{-\alpha(x-x_1)}]/k_2, & x_1 < x < x_2, \\ \mathrm{i}S\{(B'k_y - C'k_x)\cos[k_x(x-x_2)] + (B'k_x + C'k_y)\sin[k_x(x-x_2)]\}/k_1, & x_2 < x < x_3, \\ \mathrm{i}S'[D'(\alpha + k_y)\,\mathrm{e}^{-\alpha(x-x_3)}]/k_2, & x_3 < x, \end{cases} \tag{4b}$$

Here, we define $k_x = k_1\cos\theta$, $k_y = k_1\sin\theta$, $S = \mathrm{sgn}(E - V_0)$, and $S' = \mathrm{sgn}(E)$, where $\mathrm{sgn}(E - V_0)$ and $\mathrm{sgn}(E)$ are sign functions. $k_1 = |E - V_0|/\hbar v_\mathrm{F}$ and $k_2 = |E|/\hbar v_\mathrm{F}$ are wave vectors in regions II, IV and regions I, III, V respectively, and A, B, C, D, A',B', C', and D' are the undetermined coefficients of enveloping functions. Using the boundary continuity conditions of the wave functions at $x = 0$, $x = x_1$, $x = x_2$, and $x = x_3$, we can obtain

$$\boldsymbol{M}(A,B,C,D,A',B',C',D')^\mathrm{T} = 0, \tag{5}$$

where $\boldsymbol{M}(E,k_x)$ is an 8×8 matrix. The dispersion Eq. (5) is a transcendental one and cannot be solved analytically. In order to solve the equation easily, we transform Eq. (5) into $f(k_x x_1) = g(k_x x_1)$, where $f(k_x x_1)$ and $g(k_x x_1)$ are functions of $k_x x_1$. The equation $f(k_x x_1) = g(k_x x_1)$ is too long, so the analytical expression is not given here. We propose a graphical method to determine the solution of $k_x x_1$ for the guided modes. In Fig. 2, the dependencies of $f(k_x x_1)$ and $g(k_x x_1)$ on $k_x x_1$ are presented, and the intersections show the existence of the guided modes.

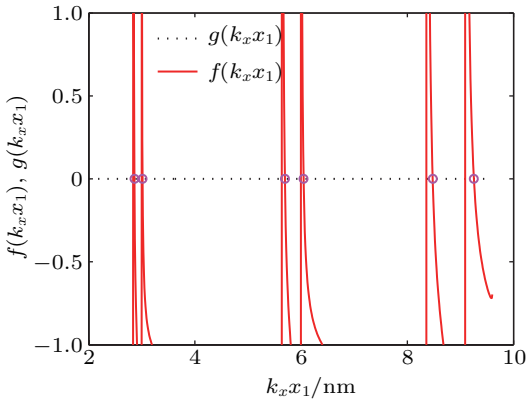


Fig. 2. (color online) Graphical determination of $k_x x_1$ for oscillating guided modes. The red solid curves and black dashed line correspond to $f(k_x x_1)$ and $g(k_x x_1)$ respectively, and the purple circles represent the location of solutions. Here the physical parameters are chosen to be $E = 15$ meV, $V_0 = 50$ meV, $x_1 = 200$ nm, $x_2 = 220$ nm, and $x_3 = 420$ nm.

3. Results and discussion

The guided modes in the double-barrier waveguides can only be supported for $0 < E < V_0/2$, when $S = \mathrm{sgn}(E - V_0) = -1$ and $S' = \mathrm{sgn}(E) = 1$. Then $SS' = -1$, which corresponds to the case of Klein tunneling. In this case, the electron makes an intraband tunneling from an electronlike to a holelike. However, the condition $SS' = 1$, corresponding to the classical motion, cannot be satisfied in the double-barrier waveguides, so the guided modes cannot be generated in the classical motion case, which is different from the quantum well graphene waveguide where the incident energy should satisfy $E > V_0/2 > 0$ and the guided modes can be generated for both the Klein tunneling with $SS' = -1$ and classical motion with $SS' = 1$.[25,28,36]

The existence of the guided modes is demonstrated in Fig. 2. For such given parameters, we can see that there exist six intersections. Moreover, we could get $k_x x_1$ from the graph directly. The corresponding values of $k_x x_1$ are 2.8613, 3.0152, 5.6954, 6.0477, 8.4775, and 9.2539, which determine six specific incident angles.

The wave function corresponding to the intersections is represented in Fig. 3. It is demonstrated that the number of the nodes of the guided modes ϕ begins from one and is order-producing with the decreasing angle. Similar to the optical waveguide terminology, we define the guide modes by the number of the nodes of the spinor wave function. In the case of Klein tunneling, the properties of guided modes in the double-barrier waveguides are quite different from that in the single barrier waveguide. It shows that only three guided modes can propagate in the single barrier waveguide for the same parameters,[24] while in the double-barrier waveguide, there are six guided modes. It means that the single-barrier modes split into symmetric and antisymmetric modes with different incident angles and x-direction energies. Two resonant wave functions in adjacent quantum barriers are mixed by tunneling and split into a doublet.

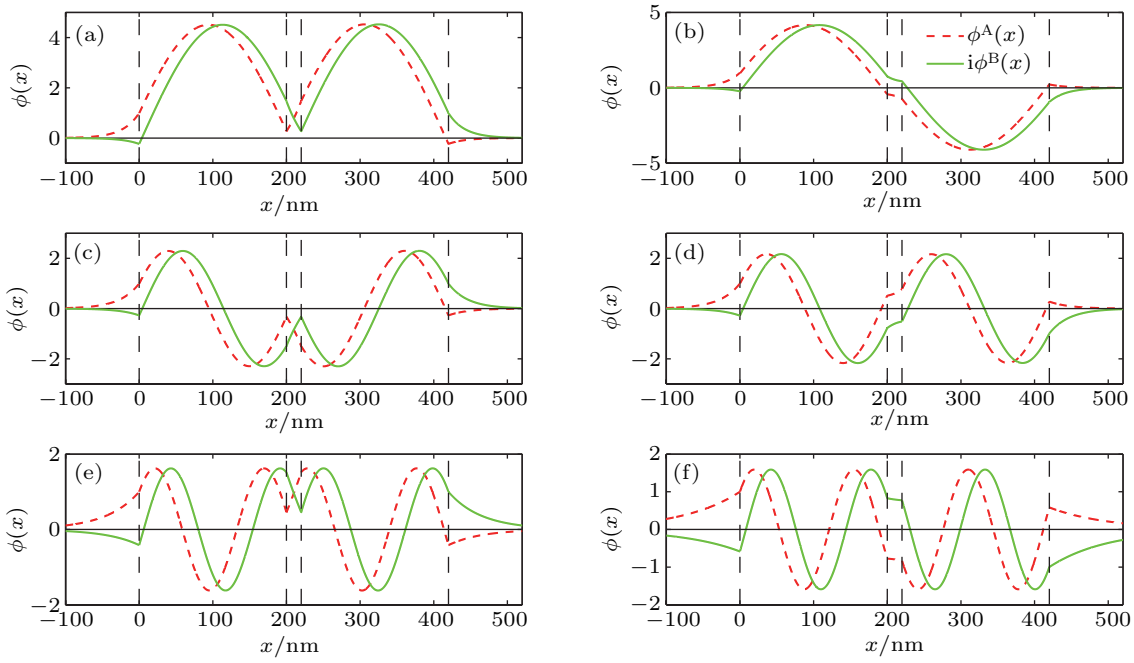


Fig. 3. (color online) The wave functions of guided modes as a function of distance of graphene waveguide, corresponding to the intersections in Fig. 2. The red dashed curve and the green solid curve correspond to $\phi^{\mathrm{A}}(x)$ and $\mathrm{i}\phi^{\mathrm{B}}(x)$, respectively. The vertical dashed line represents boundaries of the waveguide. The physical parameters are (a) $k_x x_1 = 2.8613$, (b) $k_x x_1 = 3.0152$, (c) $k_x x_1 = 5.6954$, (d) $k_x x_1 = 6.0477$, (e) $k_x x_1 = 8.4775$, and (f) $k_x x_1 = 9.2539$.

We find that the modes are from first-order to sixth-order, and the fundamental mode does not exist. Although the order of new modes generated by splitting in the double-barrier waveguides are obviously different from each other, the angle of incidence and energy of x-direction are close to each other for the two splitting modes, such as the first-order and second-order modes. However, the difference of the angle of incidence and energy of x-direction between the two splitting modes increases with the increasing order of the modes, which is shown in Fig. 4(a). For example, the incident angles of fifth-order mode and sixth-order mode are 37.0801° and 29.4415° respectively, and the energy in x-direction is 9.0440 meV and 7.3730 meV respectively. Guided modes can exist in the graphene-based waveguide with some certain separated incident angles rather than arbitrary continuous angles, and with discrete energy in x-direction.

As reported in the previous papers,[24,25,28,36] the fundamental mode can only exist in the case of classical motion and cannot exist in the Klein tunneling case in the graphene-based waveguide. The graphene double-barrier waveguides support modes only in the case of Klein tunneling, and the fundamental mode is absent. The wave function ϕ^{A} has a peak close to the right interface between region IV and region V, while the $\mathrm{i}\phi^{\mathrm{B}}$ has a peak close to the left interface between region I and region II. The difference results from that the electron and the hole have different velocities due to the conservation of pseudo-spin of the chiral particles. [36] Figure 3 also manifests an obvious shift between the wave function ϕ^{A} and $\mathrm{i}\phi^{\mathrm{B}}$, which is due to the different phase between the electron for ϕ^{A} and that of the hole for $\mathrm{i}\phi^{\mathrm{B}}$. The electron moves toward the left interface, while the hole moves toward the right one simultaneously. This may cause a local effect, that is, electrons are more likely to locate in the left part of the double-barrier waveguides, and the holes prefer to locate in the right part of the double-barrier waveguides. Here we calculate the phase difference δ between the electron for ϕ^{A} and that of the hole for $\mathrm{i}\phi^{\mathrm{B}}$ as $\delta = \pi/2 - \theta$, where θ is the incident angle. The relationship between the phase difference δ and the order of guided modes n is shown in Fig. 4(b).

In Fig. 4(b), the phase difference δ increases with the increase of the order of guided modes n. It is chiefly because that the phase difference of the guided modes is dependent on the incident angle, and the lower-order mode corresponds to a bigger angle of the incident electron, but the higher-order mode is related to a smaller angle of the incident electron. For the splitting doublet, the phase difference is close to each other. However, the phase difference for the splitting modes increases significantly with the order of modes. It results from that the energy of electron in the x-direction also increases with the order of guided modes. The split interval of the x-direction energy and the phase difference of the splitting doublet become larger and larger with the increase of the order of the modes, as is shown in Fig. 4.

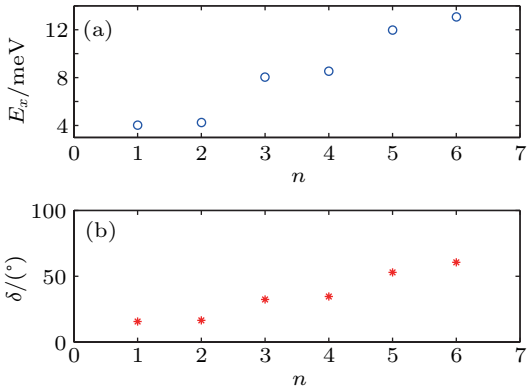


Fig. 4. (color online) The dependence of (a) x-direction energy E_x and (b) the phase difference δ on the order n of the guided modes corresponding to Fig. 3.

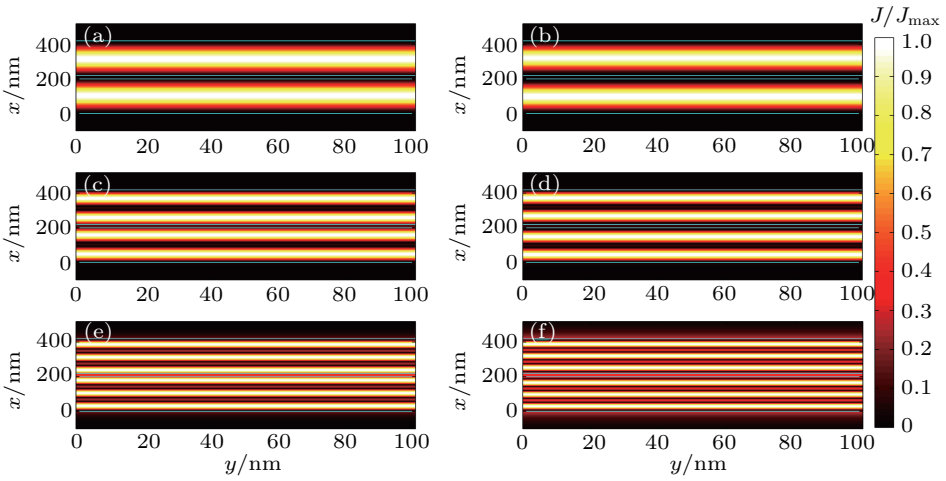


Fig. 5. (color online) The probability current densities for the six guided modes corresponding to Fig. 3. The cyan horizontal lines represent boundaries of the five regions in the waveguide.

In order to understand the confinement of the electron wave in the double-barrier waveguides, we calculate the probability current density by the definition in the Dirac equation $J_y = v_F \psi^+ \sigma_y \psi$, where $\sigma_y = \begin{pmatrix} 0 & -i \\ i & 0 \end{pmatrix}$ and $\psi = \begin{pmatrix} \phi^A(x) \\ \phi^B(x) \end{pmatrix} e^{ik_y y}$. The probability current densities for the six guided modes are shown in Fig. 5. It can be seen that the electrons can be confined in the double-barrier waveguides. Moreover, we can see that the probability current density for the first-order mode in Fig. 5(a) is quite similar to that for the second-order mode in Fig. 5(b), which are generated by modes splitting.

4. Conclusion

In conclusion, we study the guided modes in the double-barrier waveguides based on graphene. The graphene quantum double barrier can act as an electron waveguide when the incidence angle is larger than the total internal reflection critical angle. The dispersion equation, guided modes chart, wave function, phase difference, and the probability current densities are discussed in detail. It is found that electronic waves can only propagate in the graphene-based double-barrier waveguides in the case of Klein tunneling ($0 < E < V_0/2$) when the electron makes an intraband tunneling from an electronlike to a holelike.

In the double-barrier waveguide, modes splitting take place. Due to a considerable overlap of wave functions in the two barriers, the single-quantum-barrier modes split into symmetric and antisymmetric modes with different incident angles and x-direction energy. Therefore, the double-barrier waveguides can support more guided modes than single barrier waveguides do under the same circumstances. Although the incident angle and the x-direction energy in double-barrier waveguides are different from that in single barrier waveguides, but the difference is very small and can be modulated by incident energy and the electrostatic gates. It gives us a way to fine-tune some of the parameters of the guided modes in the double-barrier waveguides. Furthermore, the double-barrier waveguides have a much wider range of applications than single waveguides and have potential applications in directional couplers and the core component in future electron guided-wave integrated circuits. The split interval of x-direction energy of the doublets becomes larger and larger, and the phase difference between electrons for ϕ^A and holes for $i\phi^B$ becomes larger and larger with the increasing order of the guided modes.

In the graphene-based double-barrier waveguides, the interference and coupling effect may happen, which deserves our further investigation. The graphene-based quantum double-barrier waveguides are potentially useful in electron guided-wave integrated circuits which could perform optical-like processing. We hope these performances of graphene-based double-barrier waveguides can be helpful in designing and motivating the application of graphene-based devices in the future.

References

[1] Zhang L, Fu X L, Lei M, Chen J J, Yang J Z, Peng Z J and Tang W H 2014 *Chin. Phys. B* **23** 555
[2] Zhou P and He D W 2016 *Chin. Phys. B* **25** 770
[3] Tian H Y 2015 *Chin. Phys. B* **24** 477
[4] Huard B, Sulpizio J A, Stander N, Todd K, Yang B and Goldhaber-Gordon D 2007 *Phys. Rev. Lett.* **98** 236803
[5] Williams J R, Dicarlo L and Marcus C M 2007 *Science* **317** 638
[6] Ozyilmaz B, Jarillo-Herrero P, Efetov D, Abanin D A, Levitov L S and Kim P 2007 *Phys. Rev. Lett.* **99** 166804
[7] Castro Neto A H, Guinea F, Peres N M R, Novoselov K S and Geim A K 2009 *Rev. Mod. Phys.* **81** 109
[8] Novoselov K S, Geim A K, Morozov S V, Jiang D, Katsnelson M I, Grigorieva I V, Dubonos S V and Firsov A A 2005 *Nature* **438** 197
[9] Zhang Y, Tan Y W, Stormer H L and Kim P 2005 *Nature* **438** 201
[10] Purewal M S, Zhang Y and Kim P 2006 *Phys. Status Solidi B* **243** 3418
[11] Wang X, Cheng Z, Xu K, Tsang H K and Xu J B 2013 *Nat. Photonics* **7** 888
[12] Cheianov V V, Fal'ko V and Altshuler B L 2007 *Science* **315** 1252
[13] Beenakker C W J, Sepkhanov R A, Akhmerov A R and Tworzydlo J 2009 *Phys. Rev. Lett.* **102** 146804
[14] Gusynin V P and Sharapov S G 2005 *Phys. Rev. Lett.* **95** 146801
[15] Sharma M and Ghosh S 2011 *J. Phys. -Condens. Matter* **23** 055501
[16] Novoselov K S, McCann E, Morozov S V, Fal'ko V I, Katsnelson M I, Zeitler U, Jiang D, Schedin F and Geim A K 2006 *Nat. Phys.* **2** 177
[17] Zou J and Jin G 2011 *Appl. Phys. Lett.* **98** 122106
[18] Katsnelson M I, Novoselov K S and Geim A K 2006 *Nat. Phys.* **2** 620
[19] Croxall A F, Das Gupta K, Nicoll C A, Thangaraj M, Beere H E, Farrer I, Ritchie D A and Pepper M 2008 *Phys. Rev. Lett.* **101** 246801
[20] Deng X Q, Sun L and Li C X 2016 *Acta Phys. Sin.* **65** 068503 (in Chinese)
[21] Lu Y X and Ma N 2016 *Acta Phys. Sin.* **65** 027502 (in Chinese)
[22] Hartmann R R, Robinson N J and Portnoi M E 2010 *Phys. Rev. B* **81** 245431
[23] Myoung N, Ihm G and Lee S J 2011 *Phys. Rev. B* **83** 113407
[24] He Y, Xu Y, Yang Y and Huang W 2014 *Appl. Phys. A* **115** 895
[25] Zhang F M, He Y and Chen X 2009 *Appl. Phys. Lett.* **94** 212105
[26] Shen M, Ruan L X and Chen X 2010 *Opt. Express* **18** 12779
[27] Huang W, He Y, Yang Y and Li C 2012 *J. Appl. Phys.* **111** 053712
[28] He Y, Ding M, Yang Y and Zhang H 2015 *Superlattices Microstruct.* **85** 761
[29] Xu Y, He Y and Yang Y 2014 *Appl. Phys. A* **115** 721
[30] Yao B, Wu Y, Wang Z, Cheng Y, Rao Y, Gong Y, Chen Y and Li Y 2013 *Opt. Express* **21** 29818
[31] Williams J R, Low T, Lundstrom M S and Marcus C M 2011 *Nat. Nanotechnol.* **6** 222
[32] Hanson G W 2008 *J. Appl. Phys.* **104** 084314
[33] Gao W, Shu J, Qiu C and Xu Q 2012 *ACS Nano* **6** 7806
[34] Wu Z 2011 *Appl. Phys. Lett.* **98** 082117
[35] He Y, Huang W, Yang Y and Li C 2011 *Appl. Phys. A* **106** 41
[36] Peng P, Zhang P, Liu J K, Cao Z Z and Li G Q 2012 *Commun. Theor. Phys.* **58** 765
[37] Song Y, Wu H C and Guo Y 2012 *Appl. Phys. Lett.* **100** 253116
[38] Zhu R and Guo Y 2007 *Appl. Phys. Lett.* **91** 252113
[39] Biswas R, Mukhopadhyay S and Sinha C 2010 *Physica E* **42** 1781